Econ. Environ. Geol.
Vol. 27, No. 2, p. 191-199, 1994.

Three-Dimensional Magnetotelluric Modeling Using Integral Equations

Hee Joon Kim* and Dong Sung Lee*

ABSTRACT: We have developed an algorithm based on the method of integral equations to simulate the magnetotelluric (MT) responses of three-dimensional (3-D) bodies in a layered half-space. The inhomogeneities are divided into a number of cells and are replaced by an equivalent current distribution which is approximated by pulse basis functions. A matrix equation is constructed using the electric Green's tensor function appropriate to a layered earth, and is solved for the vector current in each cell. Subsequently, scattered fields are found by integrating electric and magnetic Green's tensor functions over the scattering current. About a 3-D conductive body near the earth's surface, interpretation using 2-D transverse electric modeling schemes can imply highly erratic low resistivities at depth. This is why these routines do not account for the effect of boundary charges. However, centrally located profiles across elongate 3-D prisms may be modeled accurately with a 2-D transverse magnetic algorithm, which implicitly includes boundary charges in its formulation. Multifrequency calculations show that apparent resistivity and impedance phase are really two complementary parameters. Hence, they should be treated simultaneously in broadband MT interpretation.

INTRODUCTION

Magnetotelluric (MT) data reflects, strictly speaking, responses from three-dimensional (3-D) resistivity structure in the earth, but traditionally they have been interpreted using 1-D and sometimes 2-D models. This tradition has arisen because 3-D modeling routines require considerable computing means to handle complex earth structure, but such means are not readily available. This shortcoming produces a lack of concensus on the interpretive errors which occur when 1-D and 2-D computational aids are used in 3-D areas.

The scattering of electromagnetic waves from 3-D resistivity structure in the earth has remained difficult to model. For over a decade, integral equation approaches have been studied by many workers (e.g., Hohmann, 1975; Das and Verma, 1982; Wannamaker et al., 1984a). They are most efficient for modeling one or a few buried prisms and have been valuable for basic physical understanding and for establishing the validity of 1-D and 2-D interpretation of field data.

This paper presents recent advances in accuracy and versatility of 3-D MT modeling using integral equations over the previous works presented by Wannamaker et al. (1984a) and Hohmann (1988). Of great importance in obtaining an accurate solution is a proper treatment of boundary charge contributions from the surface of the 3-D body as shown in Wannamaker (1991). To reduce computational cost, we employ the fast Hankel tansform algorithm (Anderson 1982; Kim and Lee, 1994) in evaluating Green's tensor integrals. The 3-D integral equation solution is verified through comparison with conventional 3-D and 2-D responses. Finally, the enhanced algorithm is used to understand the validity of 2-D interpretation assumptions over 3-D structures.

* Department of Applied Geology, National Fisheries University of Pusan, Pusan 608-737, Korea

INTEGRAL EQUATION FORMULATION

Integral Equations

Fig. 1 shows a 3-D body in an n-layered host. The body is confined to layer j in this illustration; σ_b and σ_j are the conductivities of the body and layer j, respectively. The impedivity $\hat{z}=i\omega\mu$ is assumed to be that of free space. Displacement currents are ignored in the formulation.

The electric-field integral equations for the unknown total electric and magnetic fields are given by (Newman et al., 1986)

$$E(r)=E_p(r)+(\sigma_b-\sigma_j)\int_V G_l^E(r,\ r')E(r')dv', \qquad (1)$$

and

$$H(r)=H_p(r)+(\sigma_b-\sigma_j)\int_V G_l^H(r,\ r')E(r')dv', \qquad (2)$$

where $E_P(r)$ and $H_p(r)$ are the primary electric and

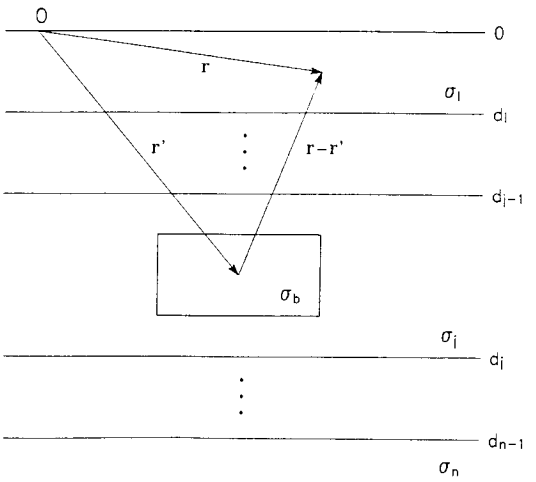

Fig. 1. Section view showing a 3-D body in a layered earth.

magnetic field at r due to plane-wave sources and 1-D earth layering. The Green's tensor functions $G_l^E(r, r')$ and $G_l^H(r, r')$ relate the electric and magnetic field, respectively, in layer l to a current element at r' in layer j, including $l=j$. The derivation of the Green's tensor functions is given by Wannamaker et al. (1984a).

Equations (1) and (2) replace the 3-D body by an equivalent scattering current distribution (Harrington, 1961). This scattering current is defined by

$$J_S(r)=(\sigma_b-\sigma_j)E(r) \tag{3}$$

where $J_S(r)$ is nonzero only over the volume of the body.

Matrix Formulation

Once the electric field in the body is known, electric and magnetic fields can be computed anywhere using equations (1) and (2). Van Bladel (1961) showed that equation (1) is also valid inside the body since a principal value of the integral exists. A matrix solution can then be constructed from equation (1) using the method of moments with pulse basis subsectional functions (Harrington, 1968).

Hohmann (1975) showed that if the 3-D body in equation (1) is divided into N cells, the total electric field at the center of the cell m due to N cells can be approximated by

$$E_b(r_m)=E_p(r_m)+\sum_{n=1}^{N}(\sigma_{bn}-\sigma_j)\Gamma_l^E(r_m;\ r_n)\cdot E_b(r_n), \tag{4}$$

where $E_b(r_m)$ is the total electric field at the center of cell m. In each cell the body conductivity σ_{bn} and total electric field are assumed to be constant and the Green's tensor function for a prism of current is defined by

$$\Gamma_l^E(r_m;\ r_n)=\int_{V_n} G_l^E(r_m,\ r')dr'. \tag{5}$$

Equation (4) can be rearranged to

$$\sum_{n=1}^{N}[(\sigma_{bn}-\sigma_j)\Gamma_l^E(r_m;\ r_n)-\delta_{m,n}]\cdot E_b(r_n)=-E_p(r_m), \tag{6}$$

where

$$\delta_{m,n}=\begin{cases} I & \text{if } m=n, \\ 0 & \text{if } m\neq n. \end{cases} \tag{7}$$

The tensors I and 0 are 3×3 identity and null tensor, respectively. Finally, considering all N values of m, a concise matrix equation is written as

$$M\cdot E_b=-E_p, \tag{8}$$

where M is the complex impedance matrix of order $3N$.

Equation (8) is solved for the total electric fields within all the cells. Once the electric field in the body is known, the electric and magnetic fields outside the body are given by discrete versions of equations (1) and (2). That is,

$$E(r)=E_p(r)+\sum_{n=1}^{N}(\sigma_{bn}-\sigma_j)\Gamma_l^E(r;\ r_n)\cdot E_b(r_n), \tag{9}$$

and

$$H(r)=H_p(r)+\sum_{n=1}^{N}(\sigma_{bn}-\sigma_j)\Gamma_l^H(r;\ r_n)\cdot E_b(r_n), \tag{10}$$

The cells representing the body need not always be cubic. In many cases the numerical solution can be improved by subdividing the body into rectangular prisms rather than cubes (Wannamaker et al., 1984a). Modifying the solution is simple, since integration of the Green's tensor function over a prism [equation (5)] can be treated as a summation of integrations over cubic subcells. Rectangular cells are useful for approximating an elongate body, provided the scattering current is polarized parallel to the strike of the body. Use of elongated cells is justified because the scattering current varies more rapidly over the short direction of the body. Newman et al. (1986) recommend, however, that cells be cubic near corners of an elongate body because variations in the scattering current are more abrupt there.

Integration of Green's Functions

Calculation of $\Gamma_l^E(r_m;\ r_n)$ comprises a great deal of

the effort in an integral equation solution. When the inhomogeneity does not cut across layer interfaces, as in Fig. 1, $l=j$ throughout in equation (6). Each cell in this case is coupled to every other cell by a Green's function composed of a primary or whole-space component $[{}^{P}\Gamma_l^E(r_m;\ r_n)]$ and a secondary or reflected component $[{}^{S}\Gamma_l^E(r_m;\ r_n)]$, i.e.,

$$\Gamma_l^E(r_m;\ r_n)={}^{P}\Gamma_l^E(r_m;\ r_n)+{}^{S}\Gamma_l^E(r_m;\ r_n). \tag{11}$$

If the body cuts across layer interface, subscripts l and j in equation (6) refer to the layers containing cells m and n, respectively. Source and field cells in different layers are coupled only by secondary Green's function; whole-space components are not given (Wannamaker et al., 1984a). Furthermore, both primary and secondary components are split into volume current and free charge contributions pertaining to the $\hat{z}_0 J_s$ and $(1/\hat{y}_j)\nabla\nabla\cdot J_s$ terms, respectively, in equation (7) of Wannamaker et al. (1984a). Such a splitting allows volume integrations of the current contribution and surface integrations of the charge contribution (Wannamaker, 1991). Surface integrations for the secondary charge Green's functions lead to the improvement over Wannamaker et al. (1984a) who implement volume integrations throughout for the secondary components.

Computational Effort

The secondary Green's functions require Hankel transformation of complicated kernel functions (Wannamaker et al., 1984a; Kim and Lee, 1994). To speed up computation, tables of the five electric and four magnetic Hankel transforms are set up prior to matrix formulation and scattered field calculation, from which specific values of Hankel transform are obtained using four-point cubic interpolation. The interpolation is one-dimensional over tables for each pair of field cell/point-source cell depth values. Wannamaker (1991) showed that in matrix calculation the 1-D interpolation is faster by a factor of 3 than the 3-D interpolation of Wannamaker et al. (1984a).

We computes the table values using the fast Hankel transform (FHT) algorithm developed by Anderson (1982). Since FHT is available for performing not only lagged but also related convolutions, the five electric and/or four magnetic Hankel transforms can be evaluated simultaneously (Kim and Lee, 1994). Moreover, by reciprocity, we know that $\Gamma_l^E(r_m;\ r_n)$ is a symmetric matrix, i.e.,

$$\Gamma_l^E(r_m;\ r_n)=\Gamma_l^E(r_n;\ r_m). \tag{12}$$

This implies that the number of elements to be calculated and stored is reduced by a factor of 2.

The computation time required to build and factor the impedance matrix can be excessive; the matrix is full, with dimensions $3N\times 3N$, where N is the number of cells. Fortunately, Tripp and Hohmann (1984) showed that the required computation time can be substantially reduced for a body with two vertical planes of symmetry. The impedance matrix for such a body is block diagonalized using the group theory (Tripp and Hohmann, 1984). The block-diagonalized matrix consists of four submatrices, each with dimension $(3N/4)\times(3N/4)$. The block-diagonalized matrix now requires one-quarter of the storage of the original matrix, and the number of operations required for matrix inversion is smaller by a factor of 12. Furthermore, the memory requirement is reduced by a factor of 16, because it is only necessary to store one of the four submatrices in memory at a time.

Apparent Resistivity and Impedance Phase

In MT work, we usually do not interpret electric and magnetic fields themselves because they depend upon the source fields over which we cannot control. Instead, we look at relationships between these fields, such as impedance tensor. It all contains information about the subsurface, however, it is very difficult to make any physical interpretation by looking directly at them. Therefore, some manipulation of the quantity is necessary to yield more recognizable parameters.

The horizontal electric and magnetic fields at the earth's surface can be related by the frequency domain expression

$$E_x=Z_{xx}H_x+Z_{xy}H_y, \tag{13}$$

and

$$E_y=Z_{yx}H_x+Z_{yy}H_y, \tag{14}$$

or in a concise form

$$E=[Z]\cdot H, \tag{15}$$

where

$$Z=\begin{pmatrix} Z_{xx} & Z_{xy} \\ Z_{yx} & Z_{yy} \end{pmatrix} \tag{16}$$

E and H are vectors formed by (E_x, E_y) and (H_x, H_y), respectively, and Z is the impedance tensor.

Apparent resistivity and impedance phase are then calculated from

$$\rho_{ij}=|Z_{ij}|^2/\mu_0\omega, \tag{17}$$

and

$$\phi_{ij}=\tan^{-1}[\mathrm{Im}(Z_{ij})/\mathrm{Re}(Z_{ij})], \quad i, j=x, y, \tag{18}$$

where $\mathrm{Im}(Z_{ij})$ and $\mathrm{Re}(Z_{ij})$ are the imaginary and real parts of Z_{ij}, respectively, and the phase ϕ_{ij} is the angle measured counterclockwise in the complex plane. Because the impedance tensor varies with respect to the coordinate system, apparent resistivity and impedance phase derived from it also vary with the coordinate system.

NUMERICAL RESULTS

Because of many possibilities for theoretical and programming errors, it is important to verify the accuracy of any numerical solution by comparing results computed by different workers. Ting and Hohmann (1981) showed surface contour maps of various MT parameters due to a 3-D prism buried in a half-space (see Fig. 10 in Ting and Hohmann, 1981), which include numerical data at some selected points. Using these numerical data, we can compare our numerical solution as shown in Figs. 2 and 3.

Figs. 2 and 3 compare ρ_{xy} and ρ_{yx}, respectively, obtained from our algorithm with corresponding Ting and Hohmann's (1981) results. Agreement between the two solutions is excellent, except for the points above center and end of the body. The lack of agreement in the points above the body is more apparent at the low frequency. The difference between two results is mainly attributed to an estimation of boundary charge contributions from the surface of the body, and they are more important at lower frequency. We believe that our results are more accurate than those of Ting and Hohmann (1981), because our method gives a better solution through a careful treatment of surface charge terms in forming the matrix and evaluating the receiver fields (Wannamaker, 1991; Kim and Lee, 1994), while Ting and Hohmann (1981) used less accurate integro-difference method.

Another useful check, and one which is enlightening for MT interpretation, is the comparison between results for elongated 3-D prisms and those for a 2-D model with same cross-section. The model used in this study is shown in Fig. 4. A conductive prism of 5 Ωm is buried in a 50 Ωm host. The size of body is 300×300 m in cross-section, and its depth is 125 m.

Since there are two vertical planes of symmetry passing through the center of the body, it is only

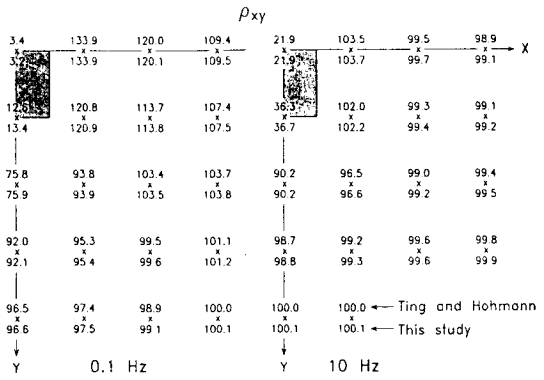

Fig. 2. Comparisons of apparent resistivities ρ_{xy} obtained from this study with corresponding Ting and Hohmann's (1981) results at 0.1 and 10 Hz.

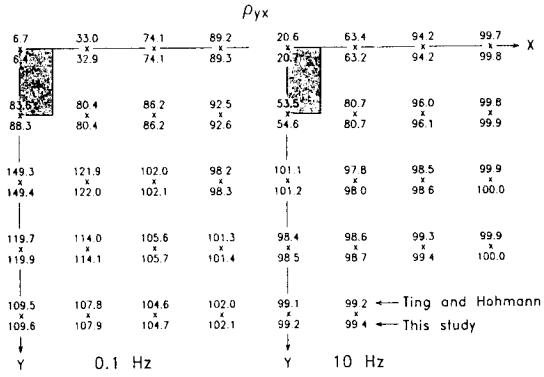

Fig. 3. Comparisons of ρ_{yx} obtained from this study with corresponding Ting and Hohmann's (1981) results.

necessary to divide one-fourth of the body into cells as shown in the plan of Fig. 4. To see how strike length of the body affects our results, we have chosen four strike lengths: 300, 450, 600 and 900 m. When the strike length is 600 m as shown in Fig. 4, for example, the total number of cells is 52.

Figs. 5 and 6 show comparisons between our 3-D results and 2-D results computed with Kim's (1990) finite-element algorithm at 32 Hz. Apparent resistivity is plotted along a profile across the center of the prism in y-axis: $x=0$. Fig. 5 shows the comparison of the incident electric field parallel to the strike direction. The 3-D results approach the 2-D curve as the strike length increases, but a significant difference still exists between the longest prism and the 2-D model. This is primarily due to an accumulation of surface charge at the boundaries perpendicular to current flow in the 3-D prism, which does not appear in the 2-D case.

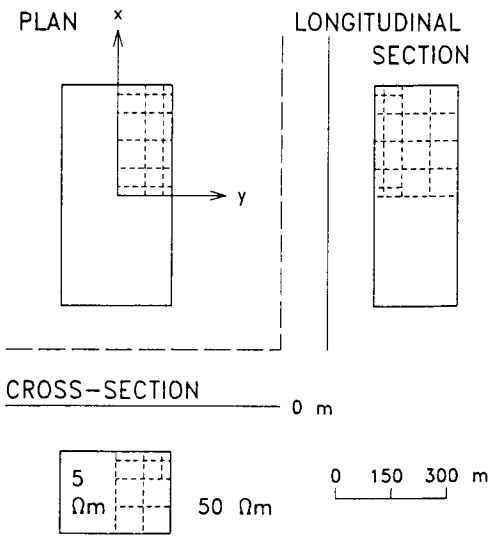

Fig. 4. Prismatic 3-D body in an uniform half-space. Dashes outline the discretization of the conductor into rectangular cells, shown only for the right half of the body in section and the upper right-hand quadrant in plan.

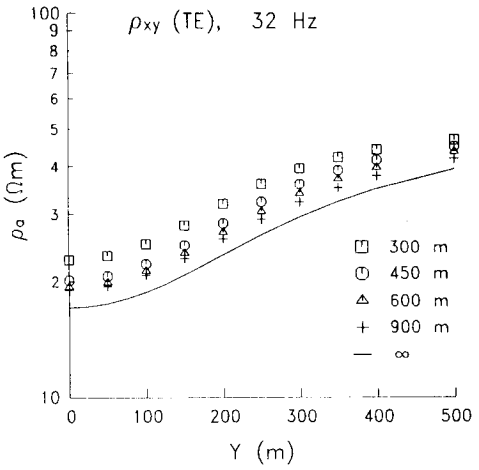

Fig. 5. Comparison of apparent resistivities ρ_{xy} between 2-D and 3-D model having different strike lengths.

Let us now briefly consider a 2-D inhomogeneity, whose strike direction corresponds to the x-axis. An x-oriented incident electric field includes only x-oriented secondary E-fields about such a structure, so that the total E-field parallels all resistivity contacts and no boundary charges exist. This is the transverse electric (TE) mode of wave polarization. At low frequencies for the TE mode, neither volume currents nor boundary charges pertain as sources for a secondary electric field.

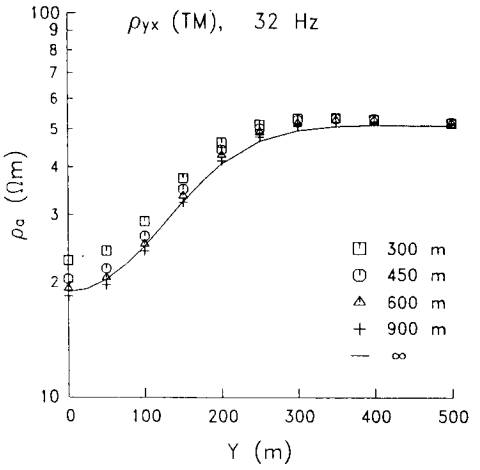

Fig. 6. Comparison of apparent resistivities ρ_{yx} between 2-D and 3-D model.

Similarly, a y-oriented incident E-field causes only y-oriented secondary E-felds over a 2-D body. Such a field polarization defines the transverse magnetic (TM) mode. However, since the incident E-field for this mode is normal to resistivity contacts in the earth, boundary charges will be induced as source for secondary E-fields. Because of boundary charges, the TM mode in the case of conductive bodies exhibits vertical current gathering (Park et al., 1983).

In the 3-D case, currents are not confined to flow parallel to strike direction as in the 2-D (TE) case, but they may be deflected laterally by regions of different conductivity. This lateral flow of current affects the nature of the fields near structures of finite extent in all three dimensions, and these effects are reflected in the calculated values.

Letting the incident E-field be perpendicular to strike direction, we obtain another comparison as shown in Fig. 6. Surface charges are included implicitly in the 2-D TM formulation, and the two solutions do not diverge as much as they do for the TE mode. As the strike length of the body decreases, an effect of limited strike length is apparent particularly in the range above the body.

Multifrequency calculations of apparent resistivity and impedance phase were performed along a profile across the center of the prism, and compared in Figs. 7~10 to calculations over a 2-D model of identical cross-section. The strike length of the prism is 900 m. For display in pseudosection form, frequency and y-axis serve as ordinate and abscissa, respectively, for contour plots of apparent resistivity and impedance

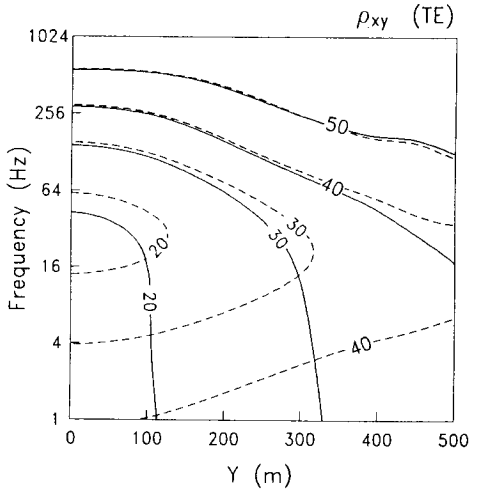

Fig. 7. Pseudosection of apparent resistivities ρ_{xy} for a profile at $x=0$ over the 3-D model with strike length of 900 m compared to 2-D TE pseudosection for corresponding model of infinite strike length. Solid and dashed contours are for 3-D and 2-D models, respectively.

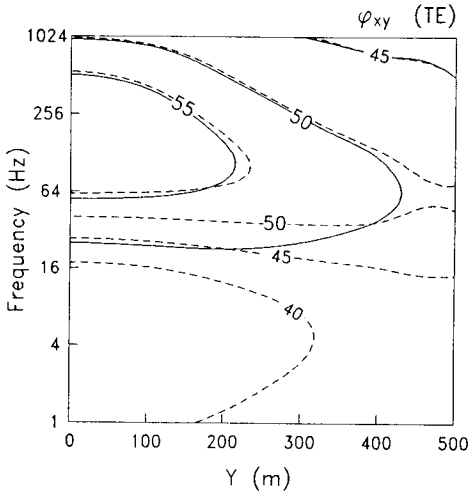

Fig. 8. Pseudosection of impedance phases ϕ_{xy} over 3-D model compared to 2-D TE model pseudosection.

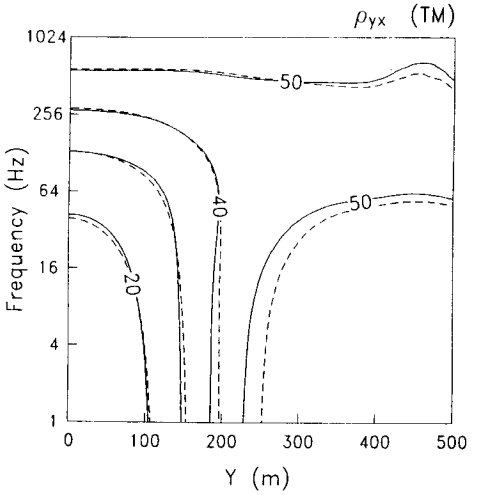

Fig. 9. Pseudosection of apparent resistivities ρ_{yx} over 3-D model compared to 2-D TM model pseudosection.

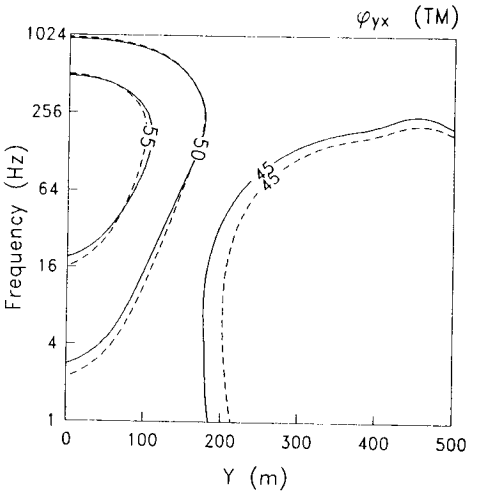

Fig. 10. Pseudosection of impedance phases ϕ_{yx} over 3-D model compared to 2-D TM model pseudosection.

phase.

A strong discrepancy between 2-D TE and corresponding 3-D responses occurs below about 64 Hz (Figs. 7 and 8). ρ_{xy} (3-D) approaches to low-frequency asymptotes as frequency falls, while ρ_{xy} (2-D) gradually increases below about 32 Hz. On the other hand, ϕ_{xy} (3-D) has nearly constant value around host impedance phase of 45° below about 16 Hz, while ϕ_{xy} (2-D) has a minimum value of 35.2° about the center of the body at 8 Hz.

This 3-D anomaly may be explained again in terms of boundary charges, acting on ρ_{xy} and ϕ_{xy}. Such charges do not occur in the 2-D body for this TE mode, so that the wave equation for $E_s(r)$ approaches the homogeneous Laplace's equation at lower frequencies and there is a diminishing contribution by the scondary E-field to the anomalous ρ_{xy} and ϕ_{xy}. Boundary charges severely depress the scattering current within the 3-D body relative to the 2-D structure. Hence, ρ_{xy} and ϕ_{xy} for the 3-D model arrive at low-frequency asymptotes around 16 Hz.

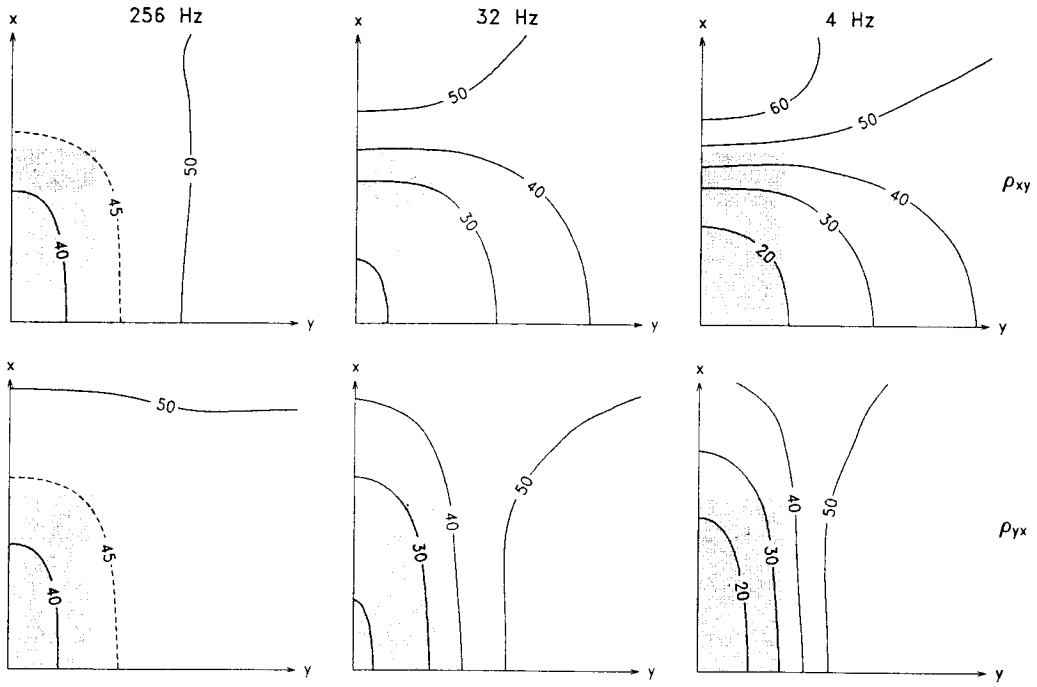

Fig. 11. Multifrequency plan maps of apparent resistivities ρ_{xy} and ρ_{yx} over upper right-hand quadrant of the body of Fig. 4.

The fact that agreement between 2-D and 3-D responses of ρ_{xy} and ϕ_{xy} is limited to high frequencies leads that 2-D TE modeling algorithms may result in erroneous resistivity cross-sections especially in deeper region. In attempting to replicate the 3-D responses in Figs. 7 and 8 with a 2-D TE routine, one would need to place false low resistivities at some depth below conductive body.

In contrast to the responses depicted in Figs. 7 and 8, anomalies in ρ_{xy} and ϕ_{xy} in Figs. 9 and 10 are essentially the same for the two 3-D traverses and 2-D profiling at all frequencies. The reasons for this agreement are twofold. First, no secondary H-field exists in the 2-D TM mode, and there is only an insignificant contribution by secondary H-fields to the corresponding 3-D response. Second, boundary charges on the sides of the body are included in both 2-D TM and 3-D formulations. These boundary charge in turn lead to current gathering into the sides of the 2-D and 3-D bodies. We infer from Figs. 9 and 10 that accurate cross-sections of earth resistivity may be interpreted from profiles of MT measurements across elongate, geometrically regular 3-D bodies using 2-D TM algorithms.

A spatial distribution of apparent resistivity signatures produced by the 3-D prism are displayed in Fig. 11. At lower frequency of 4 Hz the anomalies are roughly electric dipolar in nature, with undershoots and overshoots with respect to the host resistivity of 50 Ωm occuring over the ends of the body for ρ_{xy} and over the sides ρ_{yx}. Note also at the lower frequency that the anomalies are greater than those at 32 and 256 Hz. Boundary charges and current gathering into conductive structure cause apparent resistivities to vary spatially by a factor of 5 at 4 Hz.

Behavior of the impedance phases is entirely different from that of the apparent resistivities, as shown in Fig. 12. At 256 Hz, departures may appear in excess of 13° from the host phase of 45°. At 4 Hz, on the other hand, the secondary E-field is essentially in phase with the incident E-field and total and incident H-field are very neary equal, so that impedance phase values deviate less than 5° from the host phase.

We see stronger variation (which means higher resolving power) of impedance phase at the higher frequency in contrast to the small variation diagnostic of apparent resistivity at the higher frequency. This suggests that apparent resistivity and impedance phase are really two complementary parameters. He-

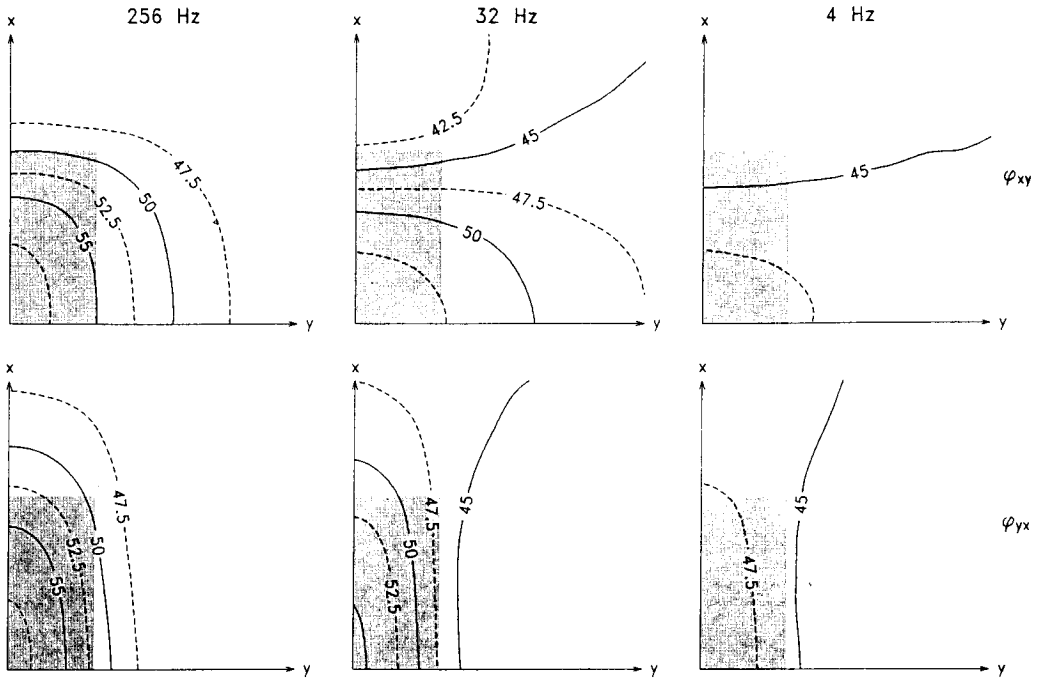

Fig. 12. Multifrequency plan maps of impedance phases ϕ_{xy} and ϕ_{yx}.

nce, they should be examined simultaneoully for any broadband MT exploration.

CONCLUSIONS

Although we developed an algorithm based on integral equation for simulating MT responses of 3-D bodies in a layered earth, we examined only the case of uniform half-space. The calculations we have shown, in addition to verifying our numercal solution, indicate that 3-D models are required for interpreting MT data.

Relative to the TE response of a 2-D body of identical cross-section, the apparent resistivity ρ_{xy} due to a conductive 3-D body suffers a widespread depression that is increasingly pronounced toward lower frequencies. This depression of the 3-D responses results from boundary charges and current gathering. Interpretation of such a 3-D response using 2-D TE modeling routines would mislead to erroneously low resistivities at depth below the true inhomogeneity. Fortunately, our model studies have shown that centrally located profiles of ρ_{yx} and ϕ_{yx} across elongate and geometrically regular 3-D prisms can be modeled accurately with a 2-D TM algorithm. Boundary charges are included in both 3-D and 2-D TM formulations. We have recognized that apparent resistivity and impedance phase are a pair of complementary parameteres. Multifrequency calculations show that behavior of the apparent resistivity is entirely different from that of the impedance phase. Hence, they should be examined simultaneouslly for any broadband MT exploration.

ACKNOWLEDGMENTS

This research was supported by the Korean Science and Engineering Foundation and the Center for Mineral Resources Research (CMR).

REFERENCES

Anderson, W. L. (1982) Fast Hankel transforms using related and lagged convolutions. ACM Trans. on Math. Software, v. 8, p. 344-368.

Das, U. C. and Verma, S. K. (1982) Electromagnetic response of an arbitrarily shaped three-dimensional conductor in a layered earth numerical results. Geophys. J. Roy. Astr. Soc., v. 68, p. 55-66.

Harrington, R. F. (1968) Field Computation by Moment Methods. MacMillan Co., 229p.

Hohmann, G. W. (1975) Three-dimensional induced polarization and electromagnetic modeling. Geophysics,

v. 40, p. 309-324.
Hohmann, G. W. (1988) Bumerical modeling for electromagnetic methods of geophyxids. In: Nabighian, M. N. (ed.) Electromagnetic methods in applied geophysics. Soc. Expl. Geophys., p. 313-363.
Kim, H. J. and Lee, D. S. (1994) Computation of Green's tensor integrals in three-dimensional magnetotelluric modeling using integral equations. Econ. Environ. Geol., v. 27, p. 41-47.
Newman, G. A., Hohmann, G. W. and Anderson, W. L. (1986) Transient electromagnetic response of a three-dimensional body in a layered earth. Geophysics, v. 51, p. 1608-1627.
Park, S. K., Orange, A. S. and Madden, T. R. (1983) Effects of three-dimensional structure on magnetotelluric sounding curves. Geophysics, v. 48, p. 1402-1405.
Tripp, A. C. and Hohmann, G. W. (1984) Block diagonalization of the electromagetic impedance matrix of a symmetric buried body using group theory. IEEE Trans. Geosci. Remote Sensing, v. GE-22, p. 62-68.
Van Bladel, J. (1961) Some remarks on Green's dyadic for infinite space. IRE Trans. Anten. Propag., v. 9, p. 561-566.
Wannamaker, P. E., Hohmann, G. W. and SanFilipo, W. A. (1984a) Electromagnetic modeling of three-dimensional bodies in layered earths using integral equations. Geophysics, v. 49, p. 60-74.
Wannamaker, P. E., Hohmann, G. W. and Ward, S. H. (1984b) Magnetotelluric responses of three-dimensional bodies in layered earths. Geophysics, v. 49, p. 1517-1533.
Wannamaker, P. E. (1991) Advances in three-dimensional magnetotelluric modeling using integral equations. Geophysics, v. 56, p. 1716-1728.

Manuscript received 21 September 1993

적분방정식을 이용한 3차원 지자기 지전류 모델링

김희준 · 이동성

요 약: 층상대지속에 있는 3차원 물체에 의한 지자기 지전류 (MT)응답을 계산하기 위하여 적분방적식을 이용한 수치모델링법을 개발하였다. 이 방법에서는 3차원 이상체를 몇 개의 세포로 분할하여 펄스기조함수로 근사할 수 있는 전류분포로 치환한다. 층상대지를 표현하는 전기 텐서그린함수를 쓰면 행렬방정식을 유도할 수 있으며 이를 각 세포의 벡터전류에 대하여 푼다. 결국 미지의 산란장은 산란전류에 관한 전기 및 자기 텐서그린함수를 적분함으로써 얻어진다. 지표면 근처에 3차원 전도성물체가 존재할 때 2차원의 TE모드 모델링으로는 깊은 곳에 가짜의 저 비저항을 가정해야 한다. 이는 TE모드 모델링에서는 경계면 전하의 영향을 고려할 수 없기 때문이다. 그러나 긴 3차원 직방체의 가운데를 가로지르는 단면은 2차원 TM모드 아르고리즘으로 정확히 모델화할 수 있으며, 이는 정식화과정에서 경계면 전하가 고려되어 있기 때문이다. 다중주파수에 관한 수치계산 결과 겉보기 비저항과 위상은 상호보완적인 변수라는 것이 밝혀졌다. 따라서 이들 변수는 주파수영역 MT 해석시 함께 취급되는 것이 바람직하다.